

# Real-Time Simulation of Grid-Connected Wind Farms Using Physical Aggregation

Vahid Jalili-Marandi, *Student Member, IEEE*, Lok-Fu Pak, and Venkata Dinavahi, *Senior Member, IEEE*

**Abstract**—The electromagnetic transient (EMT) simulation of a power system interconnected with wind farms involves such intensive computations that fully digital real-time simulators are among the effective tools for performing such simulations. To practically exploit real-time simulators for the simulation of wind farms with numerous wind turbines, the application of aggregation techniques is inevitable. In this paper, a detailed EMT model of a grid-connected wind farm with ten doubly-fed-induction-generator-based General Electric 1.5-MW wind turbines has been implemented on an advanced PC-Cluster-based real-time simulator. Three levels of physical aggregation methods are presented to reduce the computational efforts of the real-time simulation while maintaining adequate accuracy. A combination of these aggregation methods with parallel processing allowed the real-time simulation to be carried out with a fixed time step of 50  $\mu\text{s}$  and high accuracy. Various fault transient results are provided for all the aggregation levels and compared against results from the detailed wind farm model. The validity of the proposed methods and real-time simulation results has also been confirmed by comparing with offline simulation results in MATLAB/SIMULINK.

**Index Terms**—Distributed computing, power system simulation, real-time systems, wind energy.

## I. INTRODUCTION

GLOBAL WIND farms of increasing size are being established for large-scale harvesting of this abundant renewable energy resource [1], [2]. Modeling and simulation tools are essential to accurately predict the behavior of a wind farm vis-à-vis the power system [3]. An insight into the dynamic impact of a grid-connected wind farm requires comprehensive stability studies [4], [5]. Moreover, the existence of sophisticated power electronic interface for the wind farms, the testing of protection and control schemes, and the arrangement of insulation levels in wind farms involve detailed electromagnetic transient (EMT) studies.

Several commercially available simulation tools such as EMT, MATLAB/SIMULINK, and PSCAD/EMTDC provide detailed models for simulating wind farms. However, all of these simulators are offline tools which involve excessive computation time. For example, a 100-s duration of detailed

EMT simulation of a ten-turbine wind farm in MATLAB/SIMULINK, as presented in this paper, can last for several hours on a 2.8-GHz CPU. However, the same simulation on a real-time simulator will take 100 s. Another advantage of real-time simulators is their capability to communicate with real-world hardware such as digital controllers and protective relays. This feature, called hardware-in-the-loop (HIL) simulation, allows such equipment to be designed, tested, and validated under realistic system conditions before being placed in the field [6]–[9]. Practical applications that make this simulation worthy to conduct include the study of the impact of unbalanced operation, an analysis of ferroresonance in the wind farm, turbine interaction within the wind farm, and internal fault studies within the farm. Furthermore, HIL simulation can be a useful facility for training engineers.

Both fixed- and variable-speed turbines [10]–[12] have been used for wind generators; however, the doubly fed induction generators (DFIGs) have become a widely accepted design for several recent wind farm installations [13]. In [14], the *HYPERSIM* real-time simulator with 50- $\mu\text{s}$  time step was used to model one wind-turbine-driven DFIG using pulsewidth modulation converters. In [15], a real-time HIL test facility, designed for testing an all-electric ship propulsion system, was utilized for wind energy research; they have used the real-time digital simulator (*RTDS*) with a time step of 50  $\mu\text{s}$  to validate their results. In [16], a detailed real-time transient simulation for a single DFIG-based grid-connected wind turbine based on the General Electric (GE) 1.5-MW generator design has been implemented and validated on an advanced PC-Cluster-based real-time simulator. This paper presented detailed mechanical and electrical models for a single wind turbine, the control systems, and required optimization for real-time simulation. To find the most appropriate model which satisfies both accuracy and real-time constraints, several experiments were performed, and it was realized that the best configuration was the fifth-order wound rotor induction machine model with a two-mass mechanical model [17]. However, the issue that still remains unresolved is how to perform real-time simulation of large wind farms connected to the grid. Although multiple processor nodes with task partitioning might be used to perform such a simulation in real time, it certainly would not be practical if we represent a wind farm with hundreds of turbines using detailed models for individual turbines. Aggregation techniques need to be used invariably to achieve accurate real-time simulation of large wind farms. In the literature, the available offline aggregation techniques can be classified into two main groups [18], [19]: system reduction and physical aggregation methods.

Manuscript received June 26, 2009; revised September 24, 2009; accepted November 5, 2009. Date of publication December 4, 2009; date of current version August 11, 2010. This work was supported in part by the Natural Science and Engineering Research Council of Canada.

V. Jalili-Marandi and V. Dinavahi are with the Department of Electrical and Computer Engineering, University of Alberta, Edmonton, AB T6G 2V4, Canada (e-mail: v\_jalili@ece.ualberta.ca; dinavahi@ece.ualberta.ca).

L.-F. Pak is with Suncor Energy, Inc., Fort McMurray, AB T9H 3E3, Canada (e-mail: PPak@suncor.com).

Color versions of one or more of the figures in this paper are available online at <http://ieeexplore.ieee.org>.

Digital Object Identifier 10.1109/TIE.2009.2037644

In this paper, we focus on a combination of parallel processing and the physical aggregation method to achieve real-time simulation of a grid-connected wind farm. The real-time simulation was carried out with a 50- $\mu$ s time step which allows one to show the detailed switching waveforms of power electronic converters for the individual DFIG, as well as the overall dynamic response of the wind farm. In Section II, we summarize the currently available aggregation methods with their merits and drawbacks. In Section III, the structure of the power network and a wind farm with ten DFIG-based GE 1.5-MW wind turbines is shown. The performance of a detailed wind farm model without aggregation is presented in this section. In Section IV, three levels of physical aggregation using successive model reductions are applied to the wind farm, and the results are compared with the detailed wind farm model. Conclusions are presented in Section V.

## II. SUMMARY OF WIND FARM AGGREGATION METHODS

Two main groups of aggregation techniques could be identified in the literature: system reduction and physical aggregation methods. The attempt in the former is to simplify and reduce the order of the wind farm and power system models by exploiting reduction schemes. In [20], an aggregation model based on the linearization of both electrical and mechanical equations for wind turbines is proposed. This model is for power quality studies such as fluctuation of electrical and mechanical variables, and flicker. Aggregation techniques for both constant- and variable-speed wind turbines are discussed in [21]. For constant-speed turbines, it was originally proposed to sum up only the mechanical power of the single wind turbines. However, this method produced errors in the case of variable-speed wind turbines; thus, instead of the mechanical powers, only the electrical powers of the wind turbines were added. Further simplifications were considered in [21], such as the use of a constant performance coefficient ( $C_p$ ) instead of  $\hat{C}_p(\lambda, \theta)$ . The singular perturbation theory has been proposed in [18] to reduce the order of wind farms. The basis of this theory is to partition the time-varying variables of a system according to the rate of their dynamic change. The system is divided into two separate subsystems: slow and fast; the slow subsystem is solved by neglecting the fast one, and then, the fast subsystem is reintroduced to be solved in the appropriate time scale. In [18], it is explained that, in a wind farm except for rotor variables of the induction generator, other variables such as stator currents, terminal voltages, and branch currents can be included in the fast subsystem.

In the physical aggregation technique, the idea is to replace a set of wind turbines by a representative wind turbine in the wind farm simulation. The suggested method in [22] was to group wind turbines with identical operational conditions and consequently rescale the equivalents. For instance, in a wind farm with a rectangular arrangement, depending on the wind direction, a set of wind turbines existing in rows or columns was replaced with a single representative for each row or column [17]. A similar method has been used in [19], in which the wind turbines in the wind farms were divided into three groups based on the physical distances among them.

All of the aforementioned aggregation techniques were designed and implemented for offline simulations; however, their feasibility for real-time simulation is yet to be explored. The focus of this paper is on the real-time simulation of a grid-connected wind farm using the physical aggregation method. Different levels of aggregation have been achieved through the attuned utilization of wind farm physical data and electrical properties. The wind farm layout, wind direction, and correlation between the various vertically aligned wind turbines are the significant parameters for clustering wind turbines and partitioning the wind farm into several regions, as will be shown in Section IV.

## III. WIND FARM STRUCTURE AND DYNAMICS

Real-time studies on the single grid-connected wind turbine [16] have provided the fundamental building blocks and the necessary tool set for the model construction and analysis of a wind farm. To bring out the most salient characteristics of a wind farm, its electrical connections and physical attributes must be first clearly defined.

### A. Structure of the Wind Farm

As shown in Fig. 1, the ten DFIG-based wind turbines of a wind farm were electrically divided into four groups. The detailed EMT model of each wind turbine includes the complete aerodynamic, mechanical, and electrical components of the wind turbine, the back-to-back voltage source converter (VSC)-based power electronic interface, as well as the mechanical and electrical controllers of the wind turbine. Each wind turbine had its own 0.575/25-kV distribution transformer connected to the subcollector bus (cB1–cB4). Through the collector transformer, the voltage is boosted to 138-kV transmission level. At the end of the parallel circuit, the infinite bus B1 is backed by an ideal three-phase voltage source.

The geographical illustration shown in Fig. 2 indicates that the wind turbines are equally spaced on the same altitude with no surrounding obstacles. The variable wind source ( $v_w$ ) was made up of four components [23]–[25]: average speed, gust, ramp, and turbulence, as shown in Fig. 3. The average wind speed was assumed to be the same across the entire wind farm. The turbulence is a Gaussian-distributed random signal, while the wind speed nonlinearity and the geographical specifics of the wind farm land are ignored. It is, however, possible to define the turbulence in relation to the height at which the wind speed signal is of interest. In this way the geographical unevenness and nonlinearity of the wind speed can be included in the simulation [23]. In the direction shown in Fig. 2, the gust, ramp, and turbulence riding on the average wind speed would first concurrently affect wind turbines 1, 2, and 3; then 4 and 5; and so on. In order to reflect the geographical location and distance, the wind speed signals feeding to different wind turbines were individually coordinated. Since wind turbines 1, 2, and 3 were the first to be affected by the wind digressions, the wind speed pattern experienced by these three wind turbines became the modulation reference.

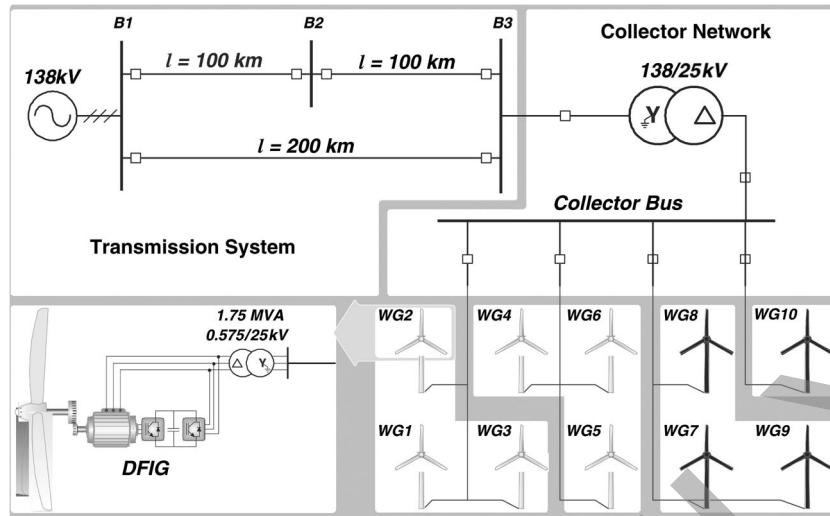


Fig. 1. Wind farm schematic.

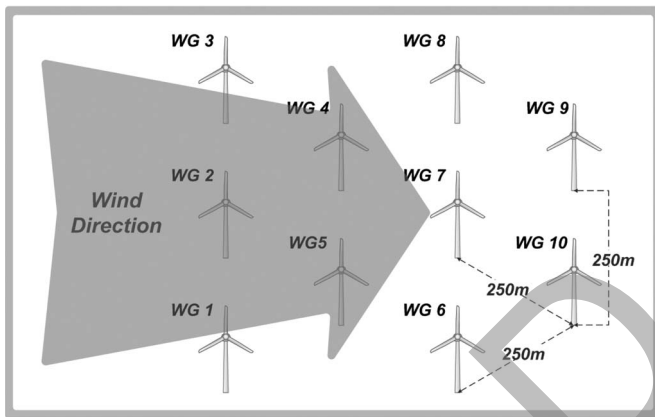


Fig. 2. Physical attributes of the wind farm and the hypothetical wind direction.

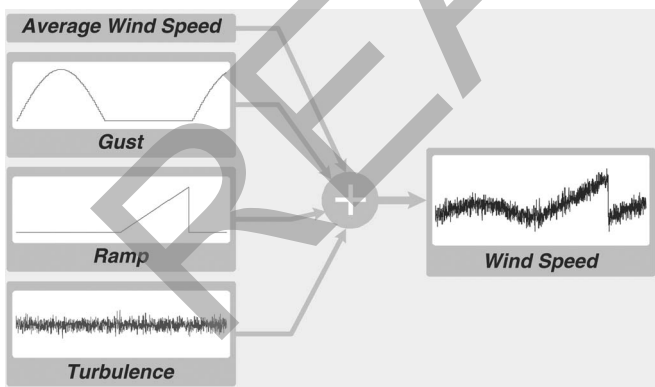


Fig. 3. Wind speed signal generation.

Referring to the physical descriptions given previously, the detailed wind farm model was developed under MATLAB/SIMULINK. Wirings internal to the wind farm were omitted mainly due to the existence of transformers (behind the wind turbines) which have a high impedance in comparison with the impedances of short-length wiring cables [21]. Nevertheless, the cables connecting the subcollector buses to the main collector bus and the transmission lines supporting the entire

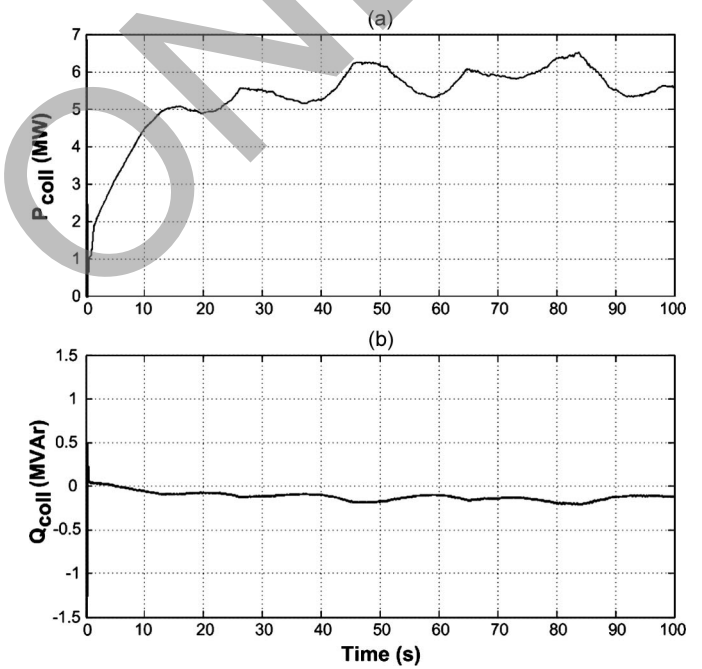


Fig. 4. Wind farm offline simulation response to variable wind speed measured at the collector bus: (a) generated active power and (b) generated reactive power from the wind farm.

wind farm were represented with the conventional distributed parameter line model. The line sections between the collector and subcollector buses are modeled with the 50-km distributed parameter line model. Although the line length and the impedances associated with the line may not reflect the real-world situation, the practice is considered valid for the study of real-time simulation realization and aggregation technique development; these will be more discussed in the next section.

For the 100-s offline simulation, all the wind turbines were initialized under exactly the same conditions. The control objective for the wind turbines was to produce maximum active power at unity power factor. The simulation time step was fixed to 50  $\mu$ s. As the aggregated behavior of the wind farm is more important, the active ( $P_{coll}$ ) and reactive ( $Q_{coll}$ ) powers at the collector bus were measured and shown in Fig. 4.

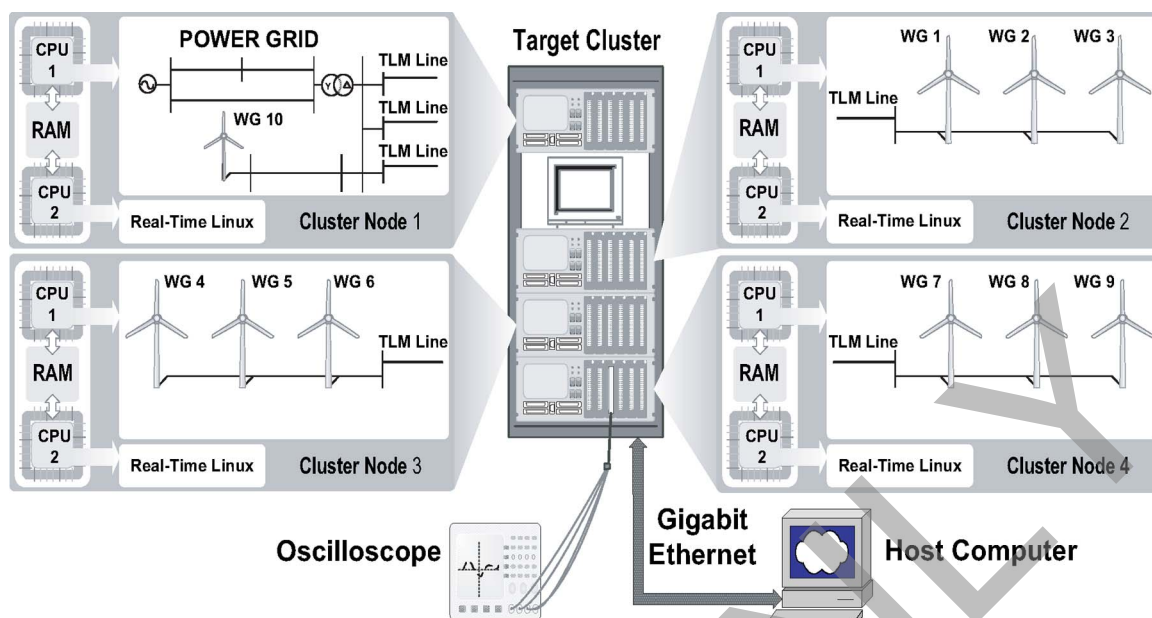


Fig. 5. Distribution of the subsystems for the wind farm model across the PC-Cluster-based real-time simulator.

The variations seen in  $P_{coll}$  are the recordings of the collective wind farm response to the wind alternations. With the given controller design, the wind turbines would only monitor and regulate the reactive power at the low-voltage side of their own distribution transformer to zero. As the internal wirings were ignored, the power factor at the subcollector buses should be very close to unity. However, the active currents flowing toward the collector bus have excited the shunt capacitances associated with the cables and, in turn, increased the generation of reactive power by small amount.

*B. Real-Time Simulation of the Wind Farm*

To complete the 100-s offline simulation in MATLAB/SIMULINK, 10 022.0 s was needed on average. One way to increase the simulation turnaround time would be to execute the model on an advanced PC-Cluster-based real-time simulator [26], [27]. Solving the wind farm model in real time required the computation power of eight 3-GHz Intel Xeon CPUs inside four shared-memory (RAM) dual-processor *cluster nodes*. Aside from speed increase, the added features from the simulator will also extend the range of investigations, such as HIL testing.

By referring to the computation time recorded for the real-time simulation of a single grid-connected wind turbine in [16], it was concluded that a maximum of three detailed wind turbine models can be simulated on a single *cluster node* with the time step fixed to 50  $\mu$ s. In order to evenly distribute the computation load across the PC Cluster, the complete wind farm was divided into four subsystems, on the PC Cluster shown in Fig. 5. Fig. 6 shows the wind farm distribution across the various subsystems which are processed in parallel on the *cluster node*. The Master subsystem contained the transmission system and one wind turbine, while the three Slave subsystems contained three wind turbines each. The communication between the Master

and Slave subsystems was established through the Bergeron transmission line model [29].

Due to the length and characteristic impedance, electrical signals sent from one end of a transmission line will be received at the other end with a time delay  $\tau$ . Because of this delay, the transmission line can be modeled as two separate yet interdependent portions. By knowing the history terms from one portion, the other portion can calculate its present state using nodal analysis. The transmission line modeling (TLM) method [30] is used to decompose the overall wind farm power system model. After splitting the transmission line model into two, one portion was retained in the Master subsystem connecting to the collector bus, and the second portion was accommodated in the Slave subsystems linking the wind turbines. The time step is small enough that the history terms from both portions were communicated to either sides just with a one time-step delay.

In theory, this model division technique should also increase the simulation speed. Since the entire electrical network was divided into four parts linked with data signals, four smaller sets of state-space matrices should be formed to represent the linear electrical components. Based on the DFIG optimization studies in [16], a smaller state-space matrix can be solved with less time. The C-code for the entire system is generated using MATLAB’s real-time workshop and compiled using OPAL-RT’s RT-LAB [31] software. After loading the executables for the four subsystems onto the PC Cluster (Fig. 5), a real-time simulation of the wind farm was started, and simulation results were exported to an external oscilloscope.

The real-time wind speed signals affecting the four groups of wind turbines in the wind farm over a 100-s interval are shown in Fig. 7. As the average wind speed was set to 11.3 m/s, a 19.16-s delay was created for the forefront of the wind variations to reach the consecutive sets of wind turbines. This explains why the variations in the wind speed signals sent

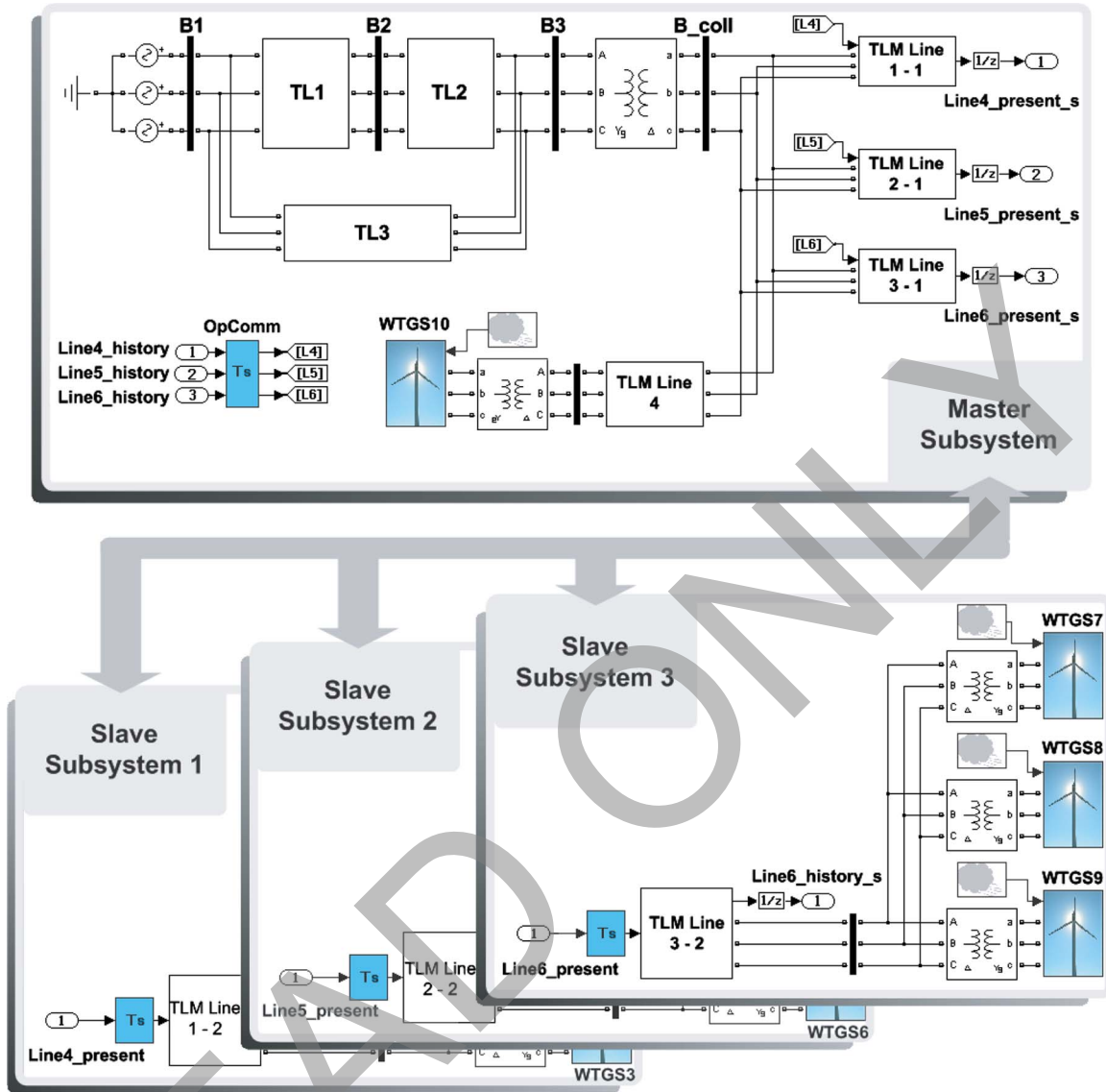


Fig. 6. Division of the detailed wind farm model for real-time simulation.

to wind turbines 4 and 5  $v_{w45}$  were started at  $t = 19.16$  s. Based on the same principle, the wind signals delivered to wind turbines 6, 7, and 8  $v_{w678}$  and those generated for wind turbines 9 and 10  $v_{w9X}$  were delayed by 38.32 and 57.48 s, respectively, with respect to  $v_{w123}$  as the modulation reference.

Fig. 8 shows the the active ( $P_{coll}$ ) and reactive ( $Q_{coll}$ ) powers at the collector bus that are the simulation results on the *OPAL-RT* real-time simulator. To validate the simulator results, those are superimposed on the offline simulation results in Fig. 9, which shows they are exactly the same. The detailed switching voltage and current waveforms for the stator side converter of individual DFIG in the wind farm are shown in Fig. 10. The grid interface for each wind turbine consists of two six-pulse VSCs connected back-to-back at their dc terminals with a shared buffering capacitor. In order to accurately represent the collective behavior of a six-pulse converter, a time-stamped switching function model was utilized [26], [28]. By comparing the real-time simulation results with the corresponding offline simulation results from MATLAB/SIMULINK, the model division technique was validated. The execution time performance

log for the real-time simulation is shown in Table I. While the model computation time for the individual subsystems was within the 50- $\mu$ s limit, the last row of Table I shows that the time step has overrun the 50- $\mu$ s limit. Because the simulator needed more time to finish the necessary computations and communications, the time step was automatically expanded. It was obvious that the communication overhead was the main cause for the overruns.

As the intensive computation has already pushed the *cluster nodes* executing the slave subsystems close to the time limit, not enough margin is left to handle the communications. Although the situation can be resolved by simply enlarging the time step, a more versatile solution of wind farm aggregation is investigated in Section IV.

#### IV. WIND FARM AGGREGATION FOR REAL-TIME SIMULATION

To reduce the amount of time and computational resources needed for the real-time simulation of a wind farm, a better

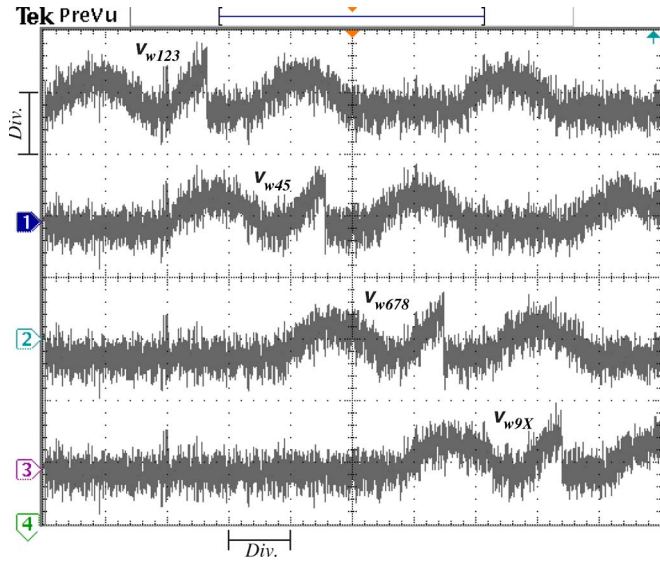


Fig. 7. Real-time oscilloscope trace of the synthesis of the variable wind speed signals for (a) wind turbines 1, 2, and 3; (b) wind turbines 4 and 5; (c) wind turbines 6, 7, and 8; and (d) wind turbines 9 and 10. ( X-axis scale) 1 Div. = 10 s. ( Y-axis scale) 1 Div. = 5.65 m/s..

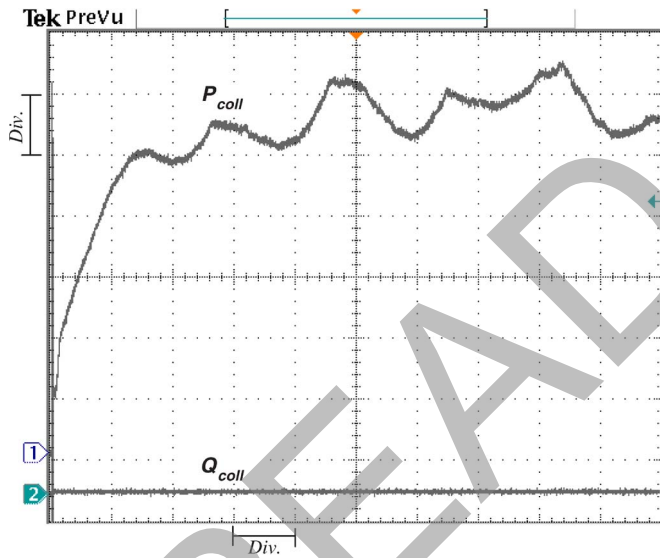


Fig. 8. Real-time oscilloscope trace of the wind farm response to variable wind speed measured at the collector bus: (a) Generated active power and (b) generated reactive power from the wind farm. (X-axis scale) 1 Div. = 10 s. (Y-axis scale) 1 Div. = 1 MW( $P$ ) and 1 MV Ar ( $Q$ ).

solution is to develop an aggregated model that is capable of representing the collective behavior of multiple or all the wind turbines. Different levels of aggregation can be achieved through attuned utilizations of the data regarding the physical attributes and electrical properties of the wind farm. In this section, three levels of aggregation are presented, and their feasibility is demonstrated for real-time simulation. The detailed wind farm model is used as a high resolution benchmark against which the results from the aggregated models were compared. Both steady-state and transient results have been considered. In the transient case, two kinds of grid faults, single-line-to-ground and three-phase-to-ground, were imposed on bus B2 shown in Fig. 1. The single-line-to-ground fault happened at

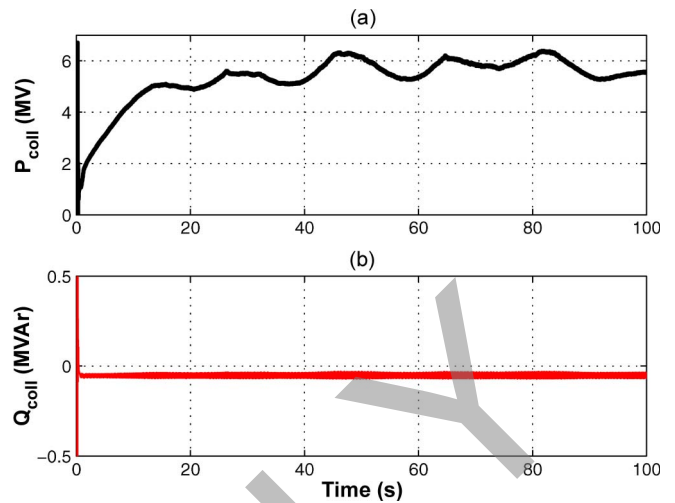


Fig. 9. Comparison of real-time results of the detailed model with the offline simulation: (a) Generated active power and (b) generated reactive power from the wind farm at the collector bus.

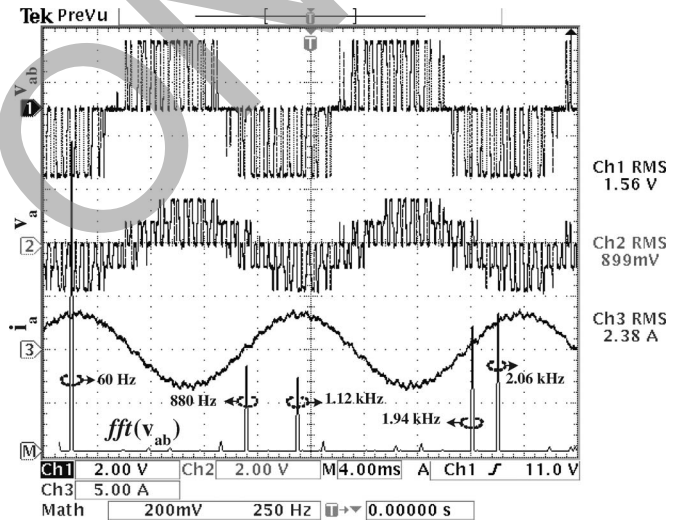


Fig. 10. Real-time oscilloscope trace of converter phase-to-phase and phase-to-ground voltages, line current, and harmonic spectrum of phase-to-phase voltage:  $v_{ab}$  V( $\times 500$ ),  $v_a$  V( $\times 500$ ),  $i_a$  A( $\times 200$ ).

$t = 10.15$  s and lasted for 9 cycles/0.15 s; after all the transients from this fault have completely settled down, a 9-cycle/0.15-s three-phase-to-ground fault was triggered at  $t = 20$  s.

### A. Level-1 Aggregation

According to the wind farm layout and wind direction given in Fig. 2, the strong correlation between the vertically aligned wind turbines allowed the division of the wind farm into four regions, as shown in Fig. 11. To represent the collective generation capacity within each region, an equivalently rated wind turbine model was utilized. For example, the replacement wind turbine model of Region 1 had a rating of 50.01 MVA ( $= 3 \times 1.67$  MVA).

The higher rating wind turbines were derived directly from the existing model with a nominal rating of 1.67 MVA. Since the wound rotor induction motor in the existing wind turbine

TABLE I  
PERFORMANCE LOG FOR THE REAL-TIME SIMULATION OF THE DETAILED WIND FARM MODEL

Time Distribution	Master ( $\mu$ s)	Slave1 ( $\mu$ s)	Slave2 ( $\mu$ s)	Slave3 ( $\mu$ s)
Computation Time	16.327	42.420	42.758	42.300
Idle Time	-2.887	0.035	0.033	0.038
Data Acquisition	1.442	1.420	1.337	1.352
Status Update	0.515	0.370	0.363	0.375
Target Request Time	0.075	0.075	0.073	0.075
Host Request Time	0.042	0.040	0.040	0.037
Synchronization	0.042	0.043	0.035	0.039
Signal To Master	-	6.338	6.432	6.178
Signal From Master	-	1.992	2.117	1.975
Signal To Slave1	6.338	-	-	-
Signal From Slave1	14.768	-	-	-
Signal To Slave2	6.265	-	-	-
Signal From Slave2	0.075	-	-	-
Signal To Slave3	6.415	-	-	-
Signal From Slave3	0.040	-	-	-
Others	0.933	0.545	0.472	0.909
Total Step-Size	53.278	53.278	53.278	53.278

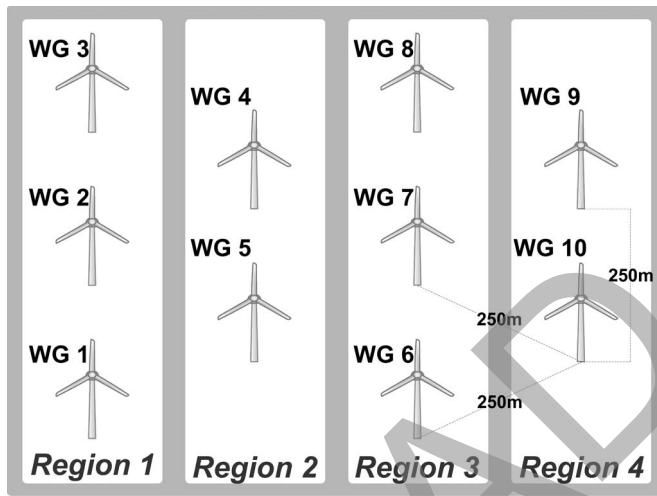


Fig. 11. Division of the wind farm for level-1 aggregation.

model was specified with per-unit parameters, its output capacity can be proportionally increased by changing the base power. There was no need to change any other parameters because the replaced model must inherit the mechanical properties and the controller characteristics. The four aggregated models were directly connected to the four subcollector buses shown in Fig. 1. Since the wind speed signals shown in Fig. 7 have already accounted for the sparsity of the wind farm, they were directly applied to the four aggregated models. Due to the differences in rating, the wind speed signals  $v_{w123}$  and  $v_{w678}$  were applied to the aggregated wind turbines representing Regions 1 and 3, respectively, while the wind speed signals  $v_{w45}$  and  $v_{w9X}$  were applied to the wind turbines representing Regions 2 and 4, respectively.

By grouping and replacing the wind turbines experiencing similar wind variations with an equivalent model, the average offline simulation time was halved to 5542.0 s. Comparisons of the simulation results accredited the aggregation technique. At the collector bus, the variable wind speed responses generated by the aggregation model were very close to those produced using the detailed wind farm model. Using the following, the

maximum discrepancies in the collector bus active and reactive power waveforms were found to be 0.92% and 3.70%, respectively (Table II):

$$\epsilon_p = \frac{\max(P_{\text{detailed}} - P_{\text{agg.}})}{P_{\text{detailed}}} \quad (1)$$

$$\epsilon_Q = \frac{\max(Q_{\text{detailed}} - Q_{\text{agg.}})}{Q_{\text{detailed}}} \quad (2)$$

where  $P_{\text{detailed}}$  and  $Q_{\text{detailed}}$  were defined as the collector bus active and reactive powers generated using the detailed wind farm model, and  $P_{\text{agg.}}$  and  $Q_{\text{agg.}}$  were representing the collector bus active and reactive powers generated using the aggregated model.

Figs. 12 and 13 show the response of the aggregated and detailed wind farm models under balanced and unbalanced fault conditions. Overall, the steady-state and transient results match very well. Under the magnified views given in Figs. 12 and 13, the deviations become more obvious. For the single-line-to-ground fault (Fig. 12), the aggregated wind farm model tends to underestimate the oscillations in  $V_{\text{coll}}$  and  $I_{\text{coll}}$ . Minor dc offsets were also observed. By referring to Figs. 12 and 13, the discrepancies are better depicted as the mismatching high-frequency voltage and current components. In the enlarged views, the waveforms generated by the aggregated model could only outline those generated by the detailed wind farm model; higher frequency jitters were not closely matched.

When comparing the results for a three-phase balanced fault, it was found that the magnitudes of the post-fault power spikes were slightly exaggerated. This exaggeration was caused by the apparent mismatches in the post-fault voltage and current waveforms (Fig. 13), although the pattern and timing of the responses were still found to be very accurate. Since the third harmonic was filtered by the star-delta connection of the transformer, the fourth harmonic became the most prominent component in the voltage waveform (Fig. 13(a)). The aggregated model was able to adequately capture the dominant harmonic.

TABLE II  
OFFLINE EXECUTION TIMES AND ERRORS ASSOCIATED WITH DIFFERENT LEVELS OF AGGREGATION

Model	wind turbines	Rating (MVA)	$T_{avg}$ (s)	$\varepsilon_P$ (%)	$\varepsilon_Q$ (%)
Detailed	10	1.67	10022.0	–	–
Level-1	4	3.34 & 5.01	5542.0	0.92	3.70
Level-2	2	8.35	3330.7	2.42	6.04
Level-3	1	16.70	1942.1	8.07	8.15

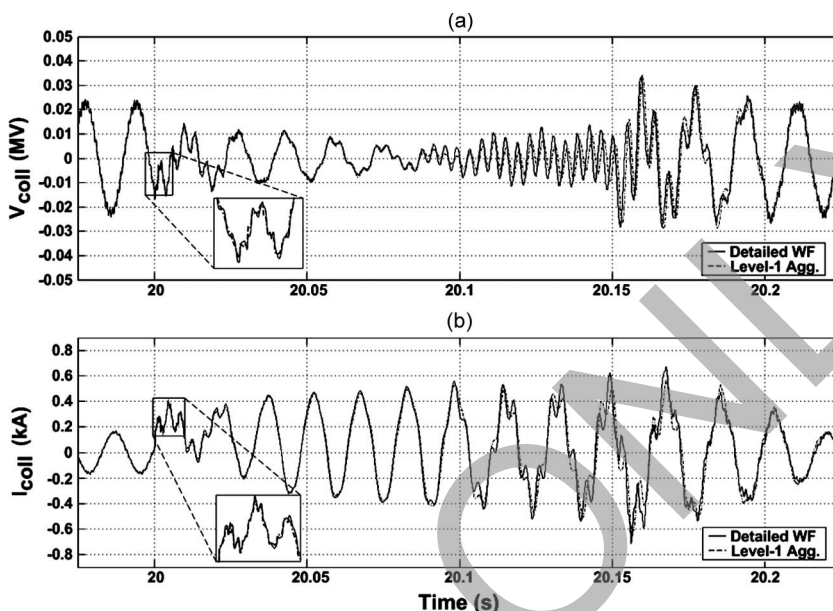


Fig. 12. Comparisons of the collector bus: phase-a (a) voltage and (b) current during the single-line-to-ground fault generated by the detailed and level-1 aggregation model.

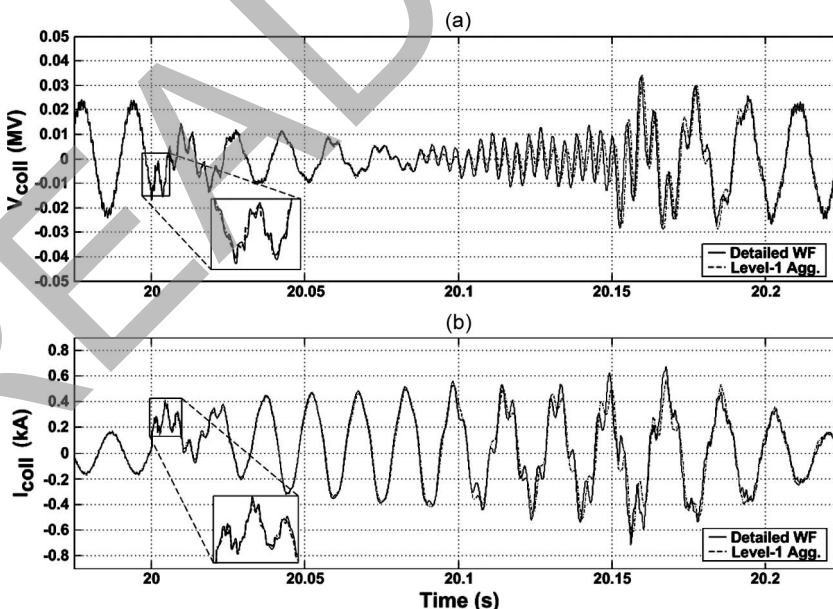


Fig. 13. Comparisons of the collector bus: phase-a (a) voltage and (b) current during the three-phase-to-ground fault generated by the detailed and level-1 aggregation model.

**B. Level-2 Aggregation**

In this level, the wind farm was divided into two parts from the middle. This setup required two equivalent wind turbine models with five times the nominal generation capacity. In order to preserve the physical attributes of the wind farm, the

wind speed signals were finely adjusted. For the first equivalent model representing wind turbines 1–5, the wind speed pattern was constructed from  $v_{w123}$  and  $v_{w45}$ . Since three of the five wind turbines should experience  $v_{w123}$  and the remaining two should experience  $v_{w45}$ , the magnitudes of the gust and ramp

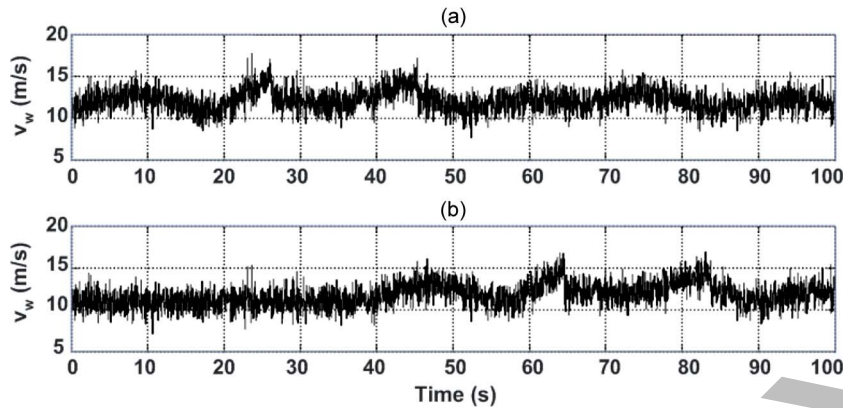


Fig. 14. Variable wind speed signals for the level-2 aggregation model.

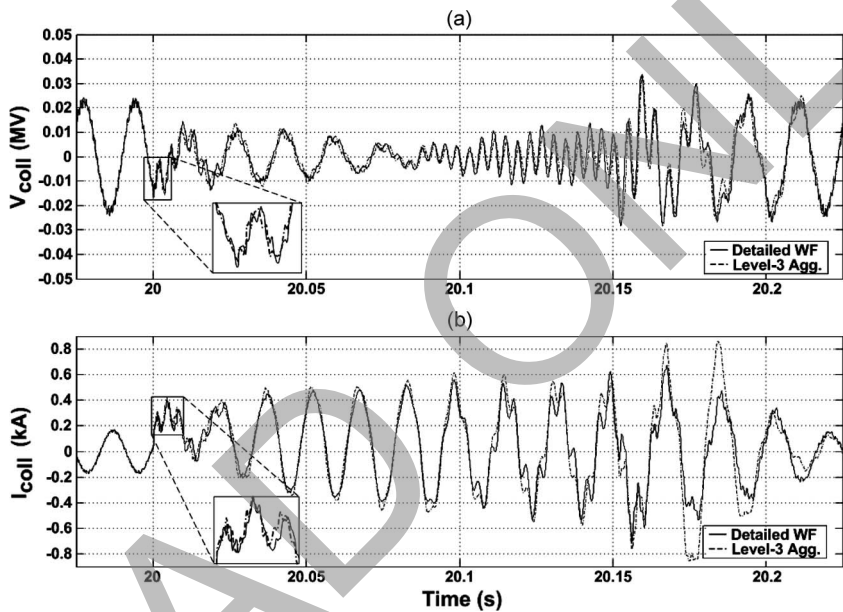


Fig. 15. Comparisons of the collector bus: phase-*a* (a) voltage and (b) current during the three-phase fault generated by the detailed and level-2 aggregation model.

were scaled accordingly while still maintaining the average wind speed at 11.3 m/s. The rescaled composite wind speed signals for *level-2* aggregation are shown in Fig. 14.

Since the entire wind farm was represented by only two equivalent wind turbines, the electrical connections at the sub-collector buses were adjusted correspondingly. Two cables were put in parallel to conserve their combined effects on power transmission.

As more details were eliminated from the wind farm model, it was expected to produce a degradation in simulation accuracy for the exchange of higher efficiency. Comparisons of the simulation results showed larger discrepancies. The maximum deviations in active and reactive powers increased to  $\varepsilon_P = 2.42\%$  and  $\varepsilon_Q = 6.04\%$  (Table II). Although the wave shapes for the fault responses were still very close to those produced by the detailed wind farm model, the exaggerated power spikes along with the enlarged dc offsets may lead to unnecessary concerns regarding the fault immunity of the wind farm.

In Fig. 15, the fault voltage and current waveform comparisons showed further disagreements for the high-frequency

components. For the three-phase fault voltage waveform (Fig. 15(a)), the amplitude differences and phase delay of the fourth harmonic component became more obvious.

### C. Level-3 Aggregation

To achieve the highest level of aggregation, all ten wind turbines were collectively represented with an equivalent model having ten times the nominal capacity. For this highly compact wind farm model, the rescaled wind pattern was synthesized from the four wind speed signals shown in Fig. 7. All the sub-collector buses were merged into one, and the cables connecting to the collector bus were combined in parallel. After a series of combinations, the wind farm was simplified to a single grid-connected wind turbine.

The simulation result comparisons showed higher discrepancies. Maximum errors  $\varepsilon_P$  and  $\varepsilon_Q$  have further increased to 8.07% and 8.15%, respectively (Table II). In the fault response comparisons (Fig. 16), the exaggeration in three-phase fault responses becomes more severe.

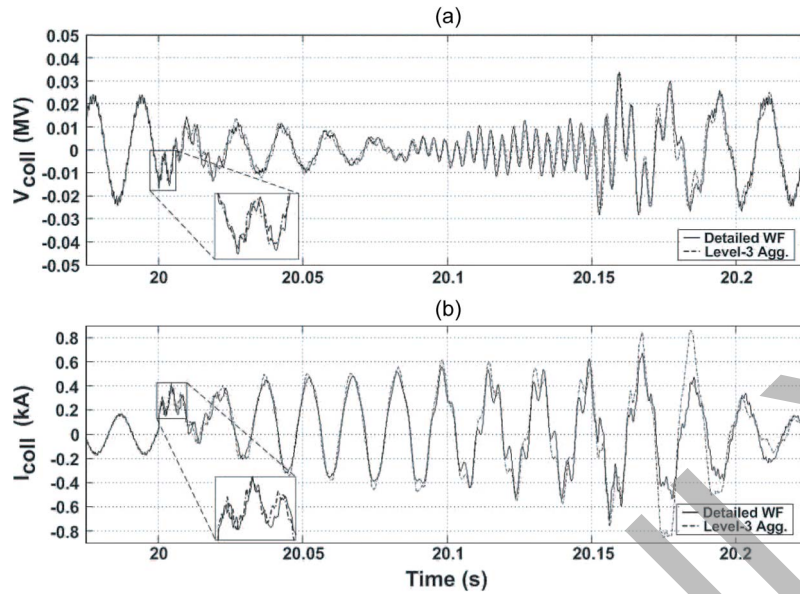


Fig. 16. Comparisons of the collector bus: phase-*a* (a) voltage and (b) current during the three-phase fault generated by the detailed and level-3 aggregation model.

*D. Aggregation Summary*

These studies conducted in the previous sections demonstrated how to effectively incorporate the electromechanical prosperities of a wind farm for aggregation purposes. In general, it was concluded that the macro behavior of the wind farm is determined by the wind speed and the geographical properties. When it comes to matching the fast transients, such as fault responses, the aggregations of the electrical network would have more substantial influence.

The achieved results for the active and reactive powers in the collector bus during different levels of aggregation have been shown in Fig. 17. When the model becomes simpler, the simulation speed and the accuracy of the simulation results correspondingly reduce, as summarized in Table II. The applications of these aggregated models should depend on the type of studies performed. All three models are considered sufficiently accurate for variable wind speed analysis and fault studies on the wind farm. When it comes to analyzing the detailed EMT response of the wind farm, the *level-1* aggregation model is generally recommended. The intermediate *level-2* aggregation model can be used to achieve the balance between simulation speed and accuracy.

*E. Real-Time Performance of the Aggregated Models*

To investigate the benefit of adopting the aggregated models for real-time simulations, the offline models were separated into subsystems. As shown in Table III, the *level-1* aggregation model required a total of three *cluster nodes* to ensure that the simulation time step ( $T_s$ ) was kept below the 50- $\mu$ s limit. However, the maximum computation  $T_{RT}$  and communication ( $T_{com}$ ) times were substantially reduced when compared with those recorded for the detailed wind farm model.

The real-time performance shown in the third row has highlighted the benefits of the *level-2* aggregation model. First,

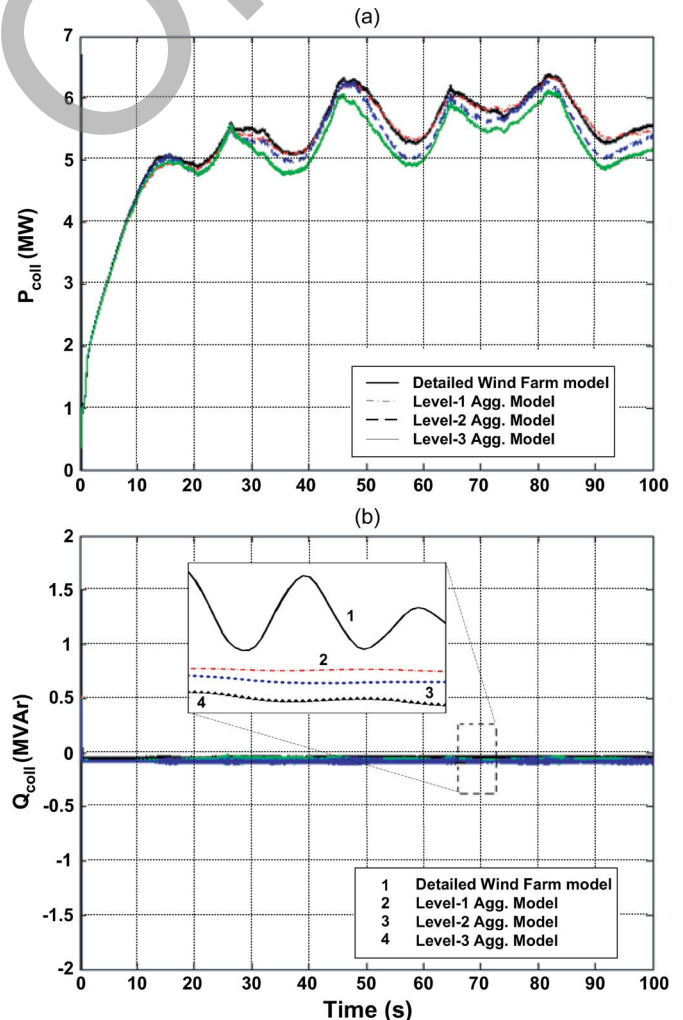


Fig. 17. Comparison of powers at the collector bus for different levels of aggregation: (a) active power and (b) reactive power.

TABLE III  
MAXIMUM EXECUTION TIMES FOR INDIVIDUAL TASKS  
WITHIN ONE TIME STEP

Model	Nodes	$T_s$ ( $\mu s$ )	$T_{RT}$ ( $\mu s$ )	$T_{com}$ ( $\mu s$ )
Detailed	4	53.278	42.758	33.901
Level-1	3	50.000	28.822	15.477
Level-2	1	50.000	30.853	–
Level-3	1	50.000	17.953	–

the number of *nodes* required for running the model in real time has drastically reduced to one. This improvement not only reduced the demand on the computational hardware but also improved the simulation performance. Since no *internode* communication was required, the 30.853- $\mu s$  computation time alone could easily fit into the 50- $\mu s$  bracket. When the accuracy was also taken into account, *level-2* aggregation model became the most suitable candidate for real-time studies of the wind farm interacting with variable wind speed and fault analysis.

Because the *level-3* aggregation model resembled a single grid-connected wind turbine, the amount of resources required for real-time simulation was the lowest among the three aggregation models. Considering the amount of time needed to develop, compile, and finally run the simulation in real-time, the *level-3* aggregation model is highly recommended for timely variable wind speed studies.

## V. CONCLUSION

Real-time digital simulation has been an effective tool for predicting wind farm behavior accurately, and more importantly, with speed, specifically when repeated simulations need to be run for long periods of time, it has been a better alternative to offline simulation. Furthermore, if an external device such as a protective relay or a digital controller needs to be tested and validated, then real-time simulation is the only recourse. The main finding of this paper is that the detailed real-time EMT simulation of realistic-size wind farms is indeed possible with the currently available off-the-shelf computer hardware. This paper has demonstrated that feasibility by simulating a grid-connected wind farm with ten DFIG-based turbines on a PC-Cluster-based real-time simulator; the wind farm model was split into various subsystems linked by transmission line models and processed in parallel on the PC-Cluster nodes. However, modeling individual wind turbines in detail is not a feasible solution, as the size of the wind farm increases due to excessive computational hardware requirement. For simulating large-scale wind farms in real time, aggregation is a better option. This paper has investigated three levels of aggregation based on the physical attributes of the wind farm. While the aggregated models varied in accuracy, from the most complex to the simplest, all of them showed a significant decrease in execution and communication times, and thus computational resources, compared with the detailed wind farm model. This opens the way for customizable aggregated models which users can configure based on the desired accuracy and speed. Having these models of the wind farm would be helpful in expediting several practical applications such as the study of the impact of unbalanced operation, the analysis of ferroresonance in the

wind farm, turbine interaction within the wind farm, and internal fault studies within the farm. Future research in this area might include a combination of various levels of aggregation based on the distances of individual turbines from the transient location and the geographical terrain.

## REFERENCES

- [1] R. Piwko, D. Osborn, R. Gramlich, G. Jordan, D. Hawkins, and K. Porter, "Wind energy delivery issues [transmission planning and competitive electricity market operation]," *IEEE Power Energy Mag.*, vol. 3, no. 6, pp. 47–56, Nov./Dec. 2005.
- [2] Industry News, "Storage Canadian winds: Wind and other projects abound," *IEEE Power Energy Mag.*, vol. 4, no. 3, pp. 86–88, May/June 2006.
- [3] E. Echenique, J. Dixon, R. Cardenas, and R. Pena, "Sensorless control for a switched reluctance wind generator, based on current slopes and neural networks," *IEEE Trans. Ind. Electron.*, vol. 56, no. 3, pp. 817–825, Mar. 2009.
- [4] S. Kim, J. Jeon, C. Cho, J. Ahn, and S. Kwon, "Dynamic modeling and control of a grid-connected hybrid generation system with versatile power transfer," *IEEE Trans. Ind. Electron.*, vol. 55, no. 4, pp. 1677–1688, Apr. 2008.
- [5] D. J. Trudnowski, A. Gentile, J. M. Khan, and E. M. Petritz, "Fixed-speed wind-generator and wind-park modeling for transient stability studies," *IEEE Trans. Power Syst.*, vol. 19, no. 4, pp. 1911–1917, Nov. 2004.
- [6] B. Lu, X. Wu, H. Figueroa, and A. Monti, "A low cost real-time hardware-in-the-loop testing approach of power electronics control," *IEEE Trans. Ind. Electron.*, vol. 54, no. 2, pp. 919–931, Apr. 2007.
- [7] G. G. Parma and V. Dinavahi, "Real-time digital hardware simulation of power electronics and drives," *IEEE Trans. Power Del.*, vol. 22, no. 2, pp. 1235–1246, Apr. 2007.
- [8] A. Bouscayrol, P. Delarue, and B. Lemaire-Semail, "Graphical description for hardware-in-the-loop simulation," in *Proc. IEEE ISIE*, Jul. 2008, pp. 2140–2145.
- [9] A. Bouscayrol, X. Guillaud, R. Teodorescu, P. Delarue, and W. Lhomme, "Energetic macroscopic representation and invasion-based control illustrated on a wind energy conversion system using hardware-in-the-loop simulation," *IEEE Trans. Ind. Electron.*, vol. 56, no. 12, pp. 4826–4835, Dec. 2009.
- [10] Y. A. Kazachkov, J. W. Feltes, and R. Zavadil, "Modeling wind farms for power system stability studies," in *Proc. IEEE Power Eng. Soc. Gen. Meeting*, Jul. 2003, vol. 3, pp. 1526–1533.
- [11] J. G. Sloopweg, S. W. H. de Hann, H. Polinder, and W. L. Kling, "Modeling wind turbines in power system dynamics simulations," in *Proc. Power Eng. Soc. Summer Meeting*, Jul. 2001, vol. 1, pp. 22–26.
- [12] M. R. Behnke and E. Muljadi, "Reduced order dynamic model for variable-speed wind turbine synchronous generator and full power conversion topology," in *Proc. Future Power Syst. Int. Conf.*, Nov. 2005, pp. 1–6.
- [13] P. Pourbeik, R. J. Koessler, and D. L. Dickmader, "Integration of large wind farms into utility grid. Part II—Performance issues," in *Proc. IEEE PES Gen. Meeting*, Jul. 13–17, 2003, vol. 3, p. 1525.
- [14] H. Le-Huy, G. Sybille, R. Gagnon, and V. Q. Do, "Real-time simulation of PWM power converters in a doubly-fed induction generator using switching-function-based method," in *Proc. IEEE IECON*, Nov. 2006, pp. 1878–1883.
- [15] H. Li, M. Steurer, S. Woodruff, K. Shi, and D. Zhang, "Development of a unified design, test, and research platform for wind energy systems based on hardware-in-the-loop real time simulation," *IEEE Trans. Ind. Electron.*, vol. 53, no. 4, pp. 1144–1151, Aug. 2006.
- [16] L.-F. Pak and V. Dinavahi, "Real-time simulation of a wind energy system based on the doubly-fed induction generator," *IEEE Trans. Power Syst.*, vol. 24, no. 3, pp. 1301–1309, Aug. 2009.
- [17] V. Akhmatov, "Analysis of dynamic behavior of electric power systems with large amount of wind power," Ph.D. dissertation, Tech. Univ. Denmark, Lyngby, Denmark, Apr. 2003.
- [18] R. M. G. Castro and J. M. Ferreira de Jesus, "A wind park reduced-order model using singular perturbations theory," *IEEE Trans. Energy Convers.*, vol. 11, no. 4, pp. 735–741, Dec. 1996.
- [19] E. Muljadi and C. P. Butterfield, "Dynamic simulation of a wind farm with variable-speed wind turbines," *Trans. Amer. Soc. Mech. Eng.*, vol. 125, no. 4, pp. 410–417, Nov. 2003.
- [20] J. C. Pider, C. J. Carrillo, and A. E. F. Lorenzo, "Probabilistic model for mechanical power fluctuation in asynchronous wind parks," *IEEE Trans. Power Syst.*, vol. 18, no. 2, pp. 761–768, May 2003.

- [21] J. G. Slootweg and W. L. Kling, "Aggregated modeling of wind parks in power system dynamics simulations," in *Proc. IEEE Power Tech. Conf.*, Jun. 2003, vol. 3, pp. 1–6.
- [22] V. Akhmatov and H. Knudsen, "An aggregate model of a grid-connected, large-scale, offshore wind farm for power stability investigations—Importance of windmill mechanical system," *Int. J. Elect. Power Energy Syst.*, vol. 24, no. 9, pp. 709–717, Nov. 2002.
- [23] J. G. Slootweg, S. W. H. de Hann, H. Polinder, and W. L. Kling, "General model for representing variable speed wind turbines in power system dynamics simulations," *IEEE Trans. Power Syst.*, vol. 18, no. 1, pp. 144–151, Feb. 2003.
- [24] R. Chedid, F. Mard, and M. Basma, "Intelligent control of a class of wind energy conversion system," *IEEE Trans. Energy Convers.*, vol. 14, no. 4, pp. 1597–1604, Dec. 1999.
- [25] J. G. Slootweg, S. W. H. de Hann, H. Polinder, and W. L. Kling, "Aggregated modeling of wind parks with variable speed wind turbines in power system dynamics simulations," in *Proc. 14th Power Syst. Comput. Conf.*, Sevilla, Spain, Jun. 2002, pp. 1–7.
- [26] L.-F. Pak, M. O. Faruque, Xin Nie, and V. Dinavahi, "A versatile cluster-based real-time digital simulator for power engineering research," *IEEE Trans. Power Syst.*, vol. 21, no. 2, pp. 455–465, May 2006.
- [27] L.-F. Pak, V. Dinavahi, G. Chang, M. Steurer, and P. F. Ribeiro, "Real-time digital time-varying harmonic modeling and simulation techniques: IEEE Task Force on harmonics modeling and simulation," *IEEE Trans. Power Del.*, vol. 22, no. 2, pp. 1218–1227, Apr. 2007.
- [28] M. O. Faruque, V. Dinavahi, and W. Xu, "Algorithms for the accounting of multiple switching events in digital simulation of power electronic systems," *IEEE Trans. Power Del.*, vol. 20, no. 2, pp. 1157–1167, Apr. 2005.
- [29] W. Scott-Meyer, *EMTP Theory Book*. Portland, OR: Bonneville Power Administration, 1984.
- [30] AS. Y. R. Hui and C. Christopoulos, "Numerical simulation of power circuits using transmission-line modeling," *Proc. Inst. Elect. Eng.*, vol. 137, no. 6, pt. A, pp. 379–384, Nov. 1990.
- [31] *RT-LAB 8 User Manual*, Opal-RT Technology Inc., Montreal, QC, Canada, 2006, pp. 1–80.



**Vahid Jalili-Marandi** (S'06) received the B.Sc. and M.Sc. degrees in power systems engineering from the University of Tehran, Tehran, Iran, in 2003 and 2005, respectively. He is currently working toward the Ph.D. degree at the University of Alberta, Edmonton, AB, Canada.

His research interests include transient stability studies, digital real-time simulations, and high-performance computations in power systems.



**Lok-Fu (Paul) Pak** received the B.Sc. degree in electrical engineering and the M.Sc. degree in electrical and computer engineering from the University of Alberta, Edmonton, AB, Canada, in 2003 and 2006, respectively.

He is currently with Suncor Energy, Inc., Fort McMurray, AB. His work is related to industrial power system modeling, study, and reliability. His research interests include renewable energy, wind turbine generation, electromagnetic transient simulation of FACTS, power electronics, and real-time

simulation of power systems.



**Venkata Dinavahi** (S'94–M'00–SM'08) received the Ph.D. degree in electrical and computer engineering from the University of Toronto, Toronto, ON, Canada, in 2000.

He is currently a Professor at the University of Alberta, Edmonton, AB, Canada. His research interests include real-time simulation of power systems and power electronic systems, large-scale system simulation, and parallel and distributed computing.

Prof. Dinavahi is a Professional Engineer in the Province of Alberta, Canada.